tertiary amide intermediate. Diethyl ether and tetrahydrofuran react to form products indicative of exclusive Co^+ insertion into the C–O bond. The processes leading to the formation of products for Co^+ and tetrahydrofuran are indicated in Scheme IV. H_2O elimination is shown to occur by first inducing the isomerization of the ether to an ene-ol. Following Co^+ insertion into the C–O bond of tetrahydrofuran, there may be attack of the carbon which is bonded to the β carbon to facilitate CH_2O elimination.

Also included in Table II are the products formed for ethylbutylamine, which appear to be typical H_2 and small-hydrocarbon eliminations. Finally, triethylamine reacts to form products analogous to diethyl ether. Co^+ readily inserts into the polar C–N bond of triethylamine.

Conclusions

The polar C–N bond in primary and secondary amines is not as susceptible to attack by transition-metal ions, as are similar polar bonds. The amine nitrogen is not a strong "directing" group for the metal. Amine reactions closely parallel alkane reactions. Co^+ reacts with the alkyl chain in larger primary amines as well as reacting by insertion into the N–H bond. The reason for failure of Co^+ to insert into the $R-NH_2$ bond may be due to the weak Co^+-NH_2 bond. There are considerable parallels in condensed phases which indicate that primary amide complexes are not easily formed.

Studies of this type involving gas-phase organometallic chemistry under mass spectrometric conditions are providing chemists with a unique view of the interaction of metal centers with organic molecules. Molecules representative of *all* of the basic organic functional groups have not yet been studied. The work done to date indicates that metal ions react in specific ways with organic molecules. Reaction products reflect functional group and structure. Thus, such work is also done to investigate the possibility of using metal ions as chemical ionization (CI) reagents. This concept has been pointed out previously. Reactions such as

$$CoCO^+ + M \rightarrow CoM^+ + CO$$

are common and provide molecular weight information. Table I shows that, in the case of the butylamines, reaction products carry very specific structural information. Thus, this work further supports the concept that metal ions can be used as CI reagents.

Acknowledgments are made to (1) the donors of the Petroleum Research Fund, administered by the American Chemical Society, and the Research Corporation, for support of the construction of the ion cyclotron resonance spectrometer at MSU, (2) Russ Guyer and Martin Raab for their expertise in the construction of the mechanical and electronic components of the ICR (respectively), (3) the NSF for partial support of this work under Grant CHE-8023704, and (4) The Dow Chemical Company Foundation for partial support of this work.

Registry No. $Co(CO)_3NO$, 14096-82-3; Co^+, 16610-75-6; $CoCO^+$, 28963-35-1; $Co(CO)_2^+$, 28963-34-0; $Co(CO)NO^+$, 61816-95-3; $Co(CO)_2NO^+$, 61816-96-4; $Co(CO)_3NO^+$, 52309-13-4; CH_3NH_2, 74-89-5; $CH_3CH_2NH_2$, 75-04-7; *n*-$C_3H_7NH_2$, 107-10-8; *i*-$C_3H_7NH_2$, 75-31-0; *n*-$C_4H_9NH_2$, 109-73-9; *i*-$C_4H_9NH_2$, 78-81-9; *sec*-$C_4H_9NH_2$, 13952-84-6; *t*-$C_4H_9NH_2$, 75-64-9; $CH_3CH_2NHCH_2CH_3$, 109-89-7; $CH_3CH_2OCH_2CH_3$, 60-29-7; $CH_3CH_2CH_2CH_2NHCH_2CH_3$, 13360-63-9; $(CH_3CH_2)_3N$, 121-44-8; pyrrolidine, 123-75-1; tetrahydrofuran, 109-99-9; piperidine, 110-89-4.

Vertical Excited States and Magnetic Circular Dichroism Spectrum of Allene

J. Diamond and G. A. Segal*

Contribution from the Department of Chemistry, University of Southern California, Los Angeles, California 90089-0482. *Received May 12, 1983*

Abstract: Large-scale ab initio calculations of the excited singlet states of allene are reported. Excellent agreement between optical absorption data and calculated vertical transition energies and oscillator strengths is noted. The experimental magnetic circular dichroism (MCD) spectrum has no dispersive signals characteristic of degenerate excited states. We find all degenerate states to have small magnetic moments and large *B* terms, and thus would have nondispersive MCD line shapes. Calculated MCD parameters provide a novel interpretation of the MCD spectrum in the 180–155-nm region.

Allene (1,2-propadiene) is the most primitive of the cumulenes. The molecular point group in the ground-state geometry is D_{2d}. Electronic excited states of ^1E symmetry are therefore susceptible to Jahn–Teller distortion as are the ^2E states of the positive ion. There is general agreement that the highest occupied molecular orbital is a π orbital of e symmetry; one would therefore expect that a number of low-lying excited electronic states of ^1E symmetry should exist. The magnetic circular dichroism (MCD) of allene has been measured by Fuke and Schnepp[1] in the 200–155-nm region in both the gas phase and perfluorohexane (PFH) solution. Remarkably, no disperisve signals, i.e., no *A* terms, are observed. An *A* term is the talisman of a degenerate electronic state in this experiment.[2] Baker and Turner[3] and Thomas and Thompson[4] have measured the photoionization spectrum of allene and observed two peaks of 10.02 and 10.58 eV in the first ionization band; they have assigned these peaks as the Jahn–Teller split components of the ^2E state of the molecular ion. This is a Jahn–Teller splitting of more than half an electronvolt. Robin[5] has interpreted the optical absorption spectrum of allene in terms of the components of Jahn–Teller split ^1E excited electronic states of Rydberg character. The two Rydberg series are assumed to converge to the two separate ionization limits, 10.02 and 10.58 eV. Fuke and Schnepp interpret the absence of A terms as evidence of the destruction of degeneracy through Jahn–Teller splitting in all excited ^1E states.

In a previous theoretical study of the MCD spectrum of cyclopropane[6] (a molecule whose D_{3h} molecular point group admits similar effects and whose ionization spectrum also exhibits a doubly

(1) Fuke, K.; Schnepp, O. *Chem. Phys.* **1979**, *38*, 211.
(2) Stephens, P. J. *Annu. Rev. Phys. Chem.* **1974**, *25*, 201; *J. Chem. Phys.* **1970**, *52*, 3489.
(3) Baker, C.; Turner, D. W. *Chem. Commun.* **1969**, 480.
(4) Thomas, R. K.; Thompson, H. T. *Proc. R. Soc. London, Ser. A* **1974**, *339*, 29.
(5) Robin, M. B. "Higher Excited States of Polyatomic Molecules"; Academic Press: New York, 1975; Vol. 2, pp 199–202.
(6) Goldstein, E.; Vijaya, S.; Segal, G. A. *J. Am. Chem. Soc.* **1980**, *102*, 6198.

0002-7863/84/1506-0952$01.50/0 © 1984 American Chemical Society

peaked behavior), it was found that a satisfying interpretation of the MCD and optical absorption spectrum could be obtained without reference to Jahn–Teller distortions. In that molecule, *A* terms were found to be small relative to the *B* terms of degenerate states for reasons quite unrelated to the destruction of degeneracy through molecular vibration. This paper reports a similar study of the optical absorption and MCD spectra of allene. Our aim is the determination of whether fairly extensive ab initio CI calculations at the equlibrium ground-state geometry lead to an interpretation of the absorption and MCD spectra without invocation of the Jahn–Teller effect.

There has been some ab initio work on allene. Primary interest has been focused on the ground singlet and triplet states as a function of internal rotation. This has been recently reviewed by Dykstra and Schaefer.[7] While other theoretical studies of the excited states have been performed,[8-10] no calculations using correlated wave functions within an extended basis have been performed. There has been reported only one attempt to study the excited states of allene with an extended Gaussian orbital basis set,[10] but the CI basis functions used were essentially limited to single substitutions from the closed-shell SCF ground-state configuration.

Our Gaussian basis set is of intermediate quality (double ζ plus Rydbergs). Each of the CI wave functions calculated has been extracted as an approximate eigenvector of a large Hamiltonian matrix (spanned by on the order of 400 000 spin eigenfunctions). The CI was performed with the program PEPCI described elsewhere.[11] We estimate total relative errors in calculated transition energies to be about 500–2000 cm^{-1}, adequate to the elucidation of the vertical excited electronic-state structure. We believe this, to the best of our knowledge, to be the first large-scale calculation of the excited states of allene with an extended basis. As previously intimated, our interpretation of the optical absorption and MCD spectra of allene differs significantly from others, yet is has within it a pleasing element of simplicity.

Experimental Results

The ground-state SCF occupation (D_{2d} point group) of allene is $(1a_1)^2(1b_2)^2(2a_1)^2(3a_1)^2(2b_2)^2(4a_1)^2(3b_2)^2(1e)^4(2e)^4$. Removal of an electron from the highest occupied orbital yields a ^2E state, which may be Jahn–Teller unstable. The photoionization spectrum of allene shows two peaks at 10.02 and 10.58 eV in the first ionization band. These have been assigned[3,4] to the Jahn–Teller components of the ^2E molecular ion, split by half an electron volt. On this basis, Robin[5] and Fuke and Schnepp[1] argue that the optical spectrum contains two Rydberg series split by 4500 cm^{-1} converging to each of the two observed peaks in the photoionization spectrum.

The optical spectrum was first studied in detail by Sutcliffe and Walsh,[12] using photographic plates. Rabalais et al.[13] have measured the spectrum from 4.78 to 10.2 eV. Iverson and Russell[14] have reported a moderately high resolution study from 6.2 to 10.7 eV. These were all gas-phase absorption spectra. More recently, Fuke and Schnepp have measured the absorption and MCD spectra in both the gas phase and PFH solution from 6.2 to 8.0 eV. The experimental results are summarized on Table IV.

The absorption spectrum is complex. There is a very weak structureless absorption below 6.45 eV (ϵ_{max} <300 L mol^{-1} cm^{-1}). Four distinct absorption bands are observed between 6.54 and 9 eV. The first band is weak ($\epsilon_{max} \simeq 3200$), with a maximum at 6.70 eV. Next, a strong ($\epsilon_{max} \sim 23\,000$) broad absorption covers the entire 6.95–7.85-eV range. In the third band, five distinct peaks ($\epsilon_{max} \sim 10\,000$) of roughly equal intensity are present in the 8.02–8.38-eV range. Using the spectrum measured by Rabalais et al., we have estimated the oscillator strength in this region to be about 0.12. Finally a very strong transition ($\epsilon_{max} > 15\,000$) has its onset around 8.57 eV. The first band at 6.70 eV has a width of about 3000 cm^{-1}, and the strong transition above it (6.95–7.85 eV) is quite broad, with a full width at half maximum of around 5000–6000 cm^{-1}. Each of the five peaks in the third band is narrow, with widths of about 300–600 cm^{-1}. The increasing absorption beyond 8.7 eV makes the characterization of a width for the absorption beginning at 8.57 eV difficult.

Robin[5] and Fuke and Schnepp[1] interpret the spectrum in the following way: four states ($^1A_1$, $^1B_1$, $^1A_2$, and $^1B_2$) arise from the singlet $\pi \rightarrow \pi^*$ transition in allene, only one of which ($^1B_2$) is optically allowed. Some or all of the remaining three states are observed in the very weak absorption below 6.45 eV. In the weak band around 6.70 eV, Fuke and Schnepp found an MCD signal with only (positive) B term behavior. The absence of an A term is indicative of a nondegenerate excited state. There is no corresponding MCD signal in solution. They conclude this is a transition to a nondegenerate Rydberg state and confirm Robin's assignment as the half of the $2e \rightarrow 3s$ ($^1A_1 \rightarrow {}^1E$) Rydberg state converging to the threshold at 10.0 eV. They argue that the other half of the ^1E state will be 4500 cm^{-1} higher, around 7.30 eV. The strong ($f = 0.34$) transition in the 6.95–7.85-eV band exhibits a distinctive, though diffuse and only fairly resolved, structure. This band has a striking MCD spectrum in which are present both strong (negative) *B* terms and MCD signals that do not correspond to any features in the absorption spectrum or its derivative. They again agree with Robin, assigning two states to this band: the $\pi \rightarrow \pi^*$ ($^1A_1 \rightarrow {}^1B_2$) valence transition and the other half of the $\pi \rightarrow 3s$ ($^1A_1 \rightarrow {}^1E$) Rydberg state converging to the upper threshold at 10.6 eV. Finally, Fuke and Schnepp observe a strong (positive) *B* term MCD at 7.7 eV in the gas phase, where no absorption can be seen against the background of the $\pi \rightarrow \pi^*$ transition. Although they argue this state is of valence character, Robin assigns this to the $\pi \rightarrow 3p$ Rydberg series at 7.3 eV, converging to the threshold at 10.0 eV. Fuke and Schnepp tentatively assigned this to a $\pi \rightarrow \sigma^*$ ($^1A_1 \rightarrow {}^1E$) valence transition. Finally, the band at 8.02–8.38 eV is given the assignment by Robin of $\pi \rightarrow 3p$ and $\pi \rightarrow 3d$. The strong transition at 8.6 eV is identified as the upper half of the $\pi \rightarrow 3p$ series converging to the threshold at 10.6 eV. In neither the band beginning at 8.02 eV nor the band at 8.5 eV is it clear how many electronic states are present, or what peaks are vibrational in origin.

Computational Details

Basis Set and CI. The molecular geometry of allene was assumed to be of D_{2d} symmetry with $R_{CC} = 1.308$ Å, $R_{CH} = 1.087$ Å, and $\angle$ HCH = 118.2°,[15] with the *z* axis along the carbon skeleton, the dihedral planes bisecting the *xz* and *yz* planes, and the origin at the center of mass. The atomic orbital basis used was Dunning's (9s5p/4s2p) contraction[16,17] centered on each carbon, with his (5s/1s) contraction (scaled by $2^{1/2}$) centered on each hydrogen. A full set of $n = 3$ (s, p, d) cartesian Gaussians ($\zeta_s = 0.023$, $\zeta_p = 0.021$, $\zeta_d = 0.015$) were added to the central carbon atom. The $d_{x^2+y^2+z^2}$ combination was retained. While this basis lacks polarization functions that are needed for valence excitations,[17] a similar basis was adequate in the calculation of the electronic structure of cyclopropane.[6] The basis set chosen is a reasonable compromise between flexibility and economy.

This basis generates 44 molecular orbitals. The three carbon 1s molecular orbitals were frozen, and their antibonding complements were ignored, leading to 38 transformed molecular or-

(7) Dykstra, C. E.; Schaefer III, H. F. In "The Chemistry of Ketenes, Allenes and Related Compounds"; Patai, S. Ed.; Wiley: Chichester, 1980; Part 1, p 1.
(8) Buenker, R. J. *J. Chem. Phys.* **1968**, *48*, 1368.
(9) Schaad, L. J.; Burnelle, L. A.; Dressler, K. P. *Theor. Chim. Acta* **1969**, *15*, 91.
(10) Rauk, A.; Drake, A. F.; Mason, S. F. *J. Am. Chem. Soc.* **1979**, *101*, 2284.
(11) Diamond, J.; Segal, G. A.; Wetmore, R. W., manuscript in preparation.
(12) Sutcliffe, L. H.; Walsh, A. D. *J. Chem. Phys.* **1951**, *19*, 1210; *J. Chem. Soc.* **1952**, 889.
(13) Rabalais, J. W.; McDonald, J. M.; Scherr, V.; McGlynn, S. P. *Chem. Rev.* **1971**, *71*, 73.
(14) Iverson, A. A.; Russell, B. R. *Spectrochim. Acta, Part A* **1972**, *28A*, 447.
(15) Maki, A. G.; Toth, R. A. *J. Mol. Spectrosc.* **1965**, *17*, 136.
(16) Dunning, T. H., Jr. *J. Chem. Phys.* **1970**, *53*, 2823.
(17) Dunning, T. H.; Hay, P. J. In "Modern Theoretical Chemistry"; Schaefer, H. F., Ed.; Plenum Press: New York, 1976.

Table I. SCF Orbital Properties[a]

orbital	symmetry	type	ϵ_i, au	$\langle(x^2+y^2)/2\rangle^b$	$\langle z^2\rangle^b$	$(\langle R^2\rangle)^{1/2}$ c
8-9	1e	σ (CH)	−0.6106	0.470	2.306	1.802
10-11	2e	π	−0.3754	0.480	1.410	1.540
12	$5a_1$	3s	0.0185	10.843	10.916	5.710
13	$6a_1$	$3d_{z^2}$	0.0515	7.649	18.228	5.790
14	$4b_2$	$3d_{xy}$	0.0527	13.487	5.057	5.660
15-16	3e	$3d_{(yz,xz)}$	0.0530	9.540	14.067	5.757
17	$1b_1$	$3d_{x^2-y^2}$	0.0534	14.001	4.667	5.716
18	$5b_2$	$3p_z$	0.0586	5.016	11.963	4.690
19-20	4e	$3p_{(x,y)}$	0.0600	7.394	3.847	4.317
21	$7a_1$	4s	0.1068	6.831	4.474	4.259
22-23	5e	π^*	0.1676	0.918	2.109	1.986
24	$8a_1$	σ^* (s)	0.3223	1.190	7.513	3.145
25	$6b_2$	σ^* (p_z)	0.3425	1.905	7.614	3.380
26	$7b_2$	σ^* (sp)	0.4873	1.108	2.476	2.166
27-28	6e	σ^* (CH)	0.4924	1.836	2.358	2.456

[a] Nuclear energy = 59.1221 au; electronic SCF energy = −174.9479 au. [b] Areas are in Å^2; the molecular z axis is along the C-C-C backbone. [c] Length in Å.

bitals. The total SCF energy in this basis is −115.8258 au. This may be compared with Dykstra's result[18] of −115.8303 au (at a slightly different geometry) and that of Rauk et al.,[10] −115.8302 au. Both of these calculations used larger basis sets.

Table I lists a subset of the molecular orbitals and some of their properties. As expected, the valence 1e and 2e orbitals are compact ($\langle r^2\rangle$ = 11.59 and 8.47 au^2, respectively) and anisotropic, lying mainly along the principal molecular axis. The set of 10 Rydberg orbitals (12–21) is quite diffuse, extending well beyond the nuclear framework. One notes that the $5a_1$ (3s) orbital is nearly spherical in spatial extent (although, since it is orthogonal to the filled orbitals $1a_1$–$4a_1$, its inner structure is complicated). The CI method used is discussed in detail elsewhere.[11] Briefly, it employs second-order Brillouin–Wigner perturbation theory within a large multireference configuration space, using a completely variational core (or model) space of up to 128 configurations. We believe the errors in the CI procedure to be of the order 500–1000 cm^{-1} in transition energies in calculations of this size.

The CI procedure for all excited states was identical. The D_2 (abelian) subgroup of D_{2d} was used to select configurations of appropriate D_2 symmetry from the set of all single, double, and triple excitations from the Hartree–Fock configuration.[19] All configurations highly important in any of the 10 lowest eigenvectors (estimated by some initial CI) were used to form the model space. This was typically 15–20 configurations. The model space was completed by adding all configurations with a diagonal Hamiltonian matrix element less than some relatively large value, typically 0.8 au above the Hartree–Fock energy. This ensured that all the lowest states were treated evenly. Specific parameters such as configuration space size etc. are shown in Table II. More roots were sought than were of real interest, so that stability of the method was ensured. In each root, the core vector comprised 85–90% of the final vector (core and interacting tail). While the sizes of the tail space seem large, in no case was any tail configuration significant ($|C| > 0.02$); it is the sheer weight of many small numbers that makes the tail seem more important than it really is. No significant interactions were missing from the core.

The ground state was treated in a slightly different way, since the configurations (all except the SCF) that are important to it lie rather high in energy. All single and double excitations from the leading seven terms in the ground-state vector formed the zero-order space. These seven plus 30 diagonally selected configurations were used as to select the 90 most strongly interacting configurations; this formed the core space, which comprised 87% of the final vector. Although the configuration spaces in ground and excited states are significantly different, the relative tail sizes indicate that the procedure is not biased toward or against the ground state. In addition, for the excited states, six roots were of real interest, vs. one in the ground state calculation; the configuration space in the ground state is roughly $^1/_6$th the size of the excited-state configuration spaces, so the ground- and excited-state spaces are not really inequivalent.

Table II. Configuration Space Specification

symmetry	$^1A_1 + {}^1B_1$	$^1A_2 + {}^1B_2$	$^1E(1)$	$1\,^1A_1$
core size	127	128	128	128
initially selected	21	17	20	7
diagonally selected[a]	106	111	108	121
diagonal threshold, au	0.87047	0.87859	0.86998	0.64183
no. of spatial occupations	142337	142268	142268	25527
no. of configurations	441801	441680	441680	73032
no. of interacting configurations and core	289470	293990	295069	63123
no. of roots found	11	10	10	1
CPU, s	2535	2387	2443	832

[a] For $1\,^1A_1$ (ground state), 31 were diagonally selected; another 90 were selected via second-order perturbation theory with a 38-component trial vector and a threshold of 0.00048 au.

Table III summarizes the CI results for the states of interest. Only one component of the degenerate states is shown. It is worth noting that many states are a strong admixture of both valence–Rydberg and valence–valence excitations, indicating both are essential to the description of these states. Also, the highest state, $3\,^1B_2$, has a tail of 18.1%. Although no significant tail components are present in this state, basis set inadequacies may make this state difficult to represent.

Calculation of Absorption and MCD Spectra. The decadic molar extinction coefficients, $\epsilon(\tilde{\nu})$ and $\Delta\epsilon(\tilde{\nu})$, for absorption and MCD, respectively, for a molecular undergoing a transition from a nondegenerate ground state, g, to an excited state, J may be reasonably approximated in terms of quantum-mechanical matrix elements A, B, D, and a unit-normalized line-shape function, $l(\tilde{\nu})$, $[\int_0^\infty l(\nu)\,d\tilde{\nu}] = 1$. The expressions for $\epsilon(\tilde{\nu})$ and $\Delta\epsilon(\tilde{\nu})$ are given by[2]

$$\epsilon(\tilde{\nu})/\tilde{\nu} = 108.9Dl(\tilde{\nu}) \quad (1)$$

$$\Delta\epsilon(\tilde{\nu})/\tilde{\nu} = -0.0102H(A\,dl/d\tilde{\nu} + Bl) \quad (2)$$

where H is the magnetic field strength in gauss and

$$A(g \rightarrow J) = \tfrac{1}{2}\sum_{\lambda,\lambda'} Im\{\langle g|\vec{\mu}|J\lambda\rangle x \langle J\lambda'|\vec{\mu}|g\rangle \cdot \langle J\lambda|\vec{m}|J\lambda'\rangle\} \quad (3)$$

$$B(g \rightarrow J) = \sum_{\lambda} Im\{\sum_{k\neq g} \langle g|\vec{\mu}|J\lambda\rangle x \langle J\lambda|\vec{\mu}|k\rangle \cdot \langle k|\vec{m}|g\rangle \tilde{\nu}_{kg}^{-1} + \sum_{k\neq J} \langle g|\vec{\mu}|J\lambda\rangle x \langle k|\vec{\mu}|g\rangle \cdot \langle J\lambda|\vec{m}|k\rangle \tilde{\nu}_{kJ}^{-1}\} \quad (4)$$

$$D(g \rightarrow J) = \sum_{\lambda} |\langle g|\vec{\mu}|J\lambda\rangle|^2 \quad (5)$$

In eq 3–5, the subscript λ denotes the individual components of the possibly degenerate excited state J. Also, $\vec{\mu}$ and $\vec{m}$ are the electric and magnetic dipole operators, respectively. The intermediate states k in eq 4 form a complete set of states subject to the given constraints $k \neq g$ and $k \neq j$ in the two parts of the B term expression. The coefficients in eq 1 and 2 are consistent with units of debyes and Bohr magnetons (μ_B) for the electric and magnetic dipole operator matrix elements, and energy gaps $\tilde{\nu}_{kl}$ expressed in cm^{-1}, e.g., the unit of the B term is D^2 μ_B cm.

The $A(g \rightarrow J)$ term is due to the first order Zeeman effect splitting the members of a degenerate excited state, J. It vanishes for nondegenerate excited states. One should note that it is multiplied by the derivative of the line-shape function, $dl/d\tilde{\nu}$, so that a dispersive MCD signal is indicative of a degenerate excited

(18) Dykstra, C. E. *J. Am. Chem. Soc.* **1977**, *99*, 2066.

(19) While such a large calculation is certainly not necessary, and usually not desirable, in this case it was an easy thing to do. Hamiltonian matrix element formation took only 300 CPU s (on an IBM 370/168). This configuration space is completely equivalent to generating all singles and doubles from every single excitation from the Hartree–Fock configuration. For various reasons related to the algorithm used (a variation of GUGA), it is more difficult to use a configuration space spanned by all singles and doubles from many configurations (more than 10), although this may at first seem to be the appropriate configuration space.

Table III. Configuration Interaction Results

state	$E - E_{gs}$,[a] eV	tail size, %	$\langle(x^2+y^2)/2\rangle$[b]	$\langle z^2\rangle$[b]	leading terms[c]
1^1A_1	0	12.7	−4.247	−3.228	0.9345 SCF
1^1A_2	6.566	14.4	−4.790	−3.965	$0.8329(\pi \rightarrow \pi^*) + 0.4030(\pi \rightarrow 3p)$
1^1E	6.872	10.6	−9.077	−7.344	$0.7756(\pi \rightarrow 3s) - 0.5290(\pi \rightarrow 4s)$
1^1B_1	6.921	13.9	−5.250	−4.115	$0.7885(\pi \rightarrow \pi^*) + 0.4894(\pi \rightarrow 3p)$
1^1B_2	7.445	14.5	−9.590	−5.361	$0.8852(\pi \rightarrow 3p) + 0.2665(\pi \rightarrow \pi^*)$
2^1A_1	7.609	15.9	−9.923	−5.376	$0.8905(\pi \rightarrow 3p) + 0.2180(\pi \rightarrow \pi^*)$
2^1E	7.691	15.0	−7.991	−13.264	$0.8614(\pi \rightarrow 3p_z) - 0.2706(\pi \rightarrow 3d_{xy})$
2^1A_2	7.822	14.4	−10.500	−5.552	$0.7746(\pi \rightarrow 3p) - 0.3682(\pi \rightarrow \pi^*) - 0.3473(\pi \rightarrow 3d)$
2^1B_1	7.854	14.4	−10.131	−5.497	$0.7191(\pi \rightarrow 3p) - 0.4481(\pi \rightarrow \pi^*) - 0.3721(\pi \rightarrow 3d)$
3^1E	8.200	14.0	−8.542	−23.628	$0.8243(\pi \rightarrow 3d_{z^2}) - 0.2860(\pi \rightarrow 4s) - 0.2672(\pi \rightarrow 3s)$
3^1A_1	8.314	15.6	−9.477	−10.005	$0.7179(\pi \rightarrow 3d) + 0.5733(\pi \rightarrow \pi^*)$
2^1B_2	8.339	15.7	−12.864	−15.352	$0.9181(\pi \rightarrow 3d)$
3^1A_2	8.416	14.3	−13.020	−15.420	$0.8602(\pi \rightarrow 3d) + 0.3094(\pi \rightarrow 3p)$
4^1E	8.4184	13.8	−17.837	−6.716	$0.9287(\pi \rightarrow 3d_{x^2-y^2})$
5^1E	8.4188	13.7	−17.744	−6.772	$0.8868(\pi \rightarrow 3d_{xy}) + 0.2768(\pi \rightarrow 3p_z)$
3^1B_1	8.420	14.3	−12.923	−15.203	$0.8495(\pi \rightarrow 3d) + 0.3187(\pi \rightarrow 3p)$
4^1A_1	8.529	14.8	−9.133	−9.538	$0.6780(\pi \rightarrow \pi^*) - 0.5769(\pi \rightarrow 3d) - 0.2431(\pi \rightarrow 3p)$
6^1E	8.624	14.5	−18.370	−7.067	$0.6094(\pi \rightarrow 4s) + 0.4652(\pi \rightarrow 3s) + 0.3864(\pi \rightarrow 3d_{z^2})$
3^1B_2	9.066	18.1	−6.109	−4.659	$0.8620(\pi \rightarrow \pi^*) - 0.2761(\pi \rightarrow 3p)$

[a] $E_{gs} = -116.0893$ au. [b] Total (nuclear − electronic) quadrupole charge distributions in e Å^2. Values for stripped nuclei are $\langle x^2+y^2\rangle/2 = 1.740$ e Å^2, $\langle z^2\rangle = 34.463$ e Å^2. [c] For nondegenerate states, $e \rightarrow e'$ excitations are the appropriate symmetry components (e.g., $^1A_2(\pi \rightarrow \pi^*) = 1/2^{1/2}(\pi_x \rightarrow \pi_y^* - \pi_y \rightarrow \pi_x^*)$); Rydberg orbitals without subscripts are degenerate (e.g., 3d = 3e in this basis).

state. The quantity $A(g \rightarrow J)/D(g \rightarrow J)$ represents the magnetic moment of the excited state J.

The $B(g \rightarrow J)$ term, on the other hand, is in principle nonzero for all optically allowed states. It is due to the second-order mixing of the ground and excited states with all other states due to the presence of the magnetic field (the second-order Zeeman effect). Since the B term contains an infinite sum over intermediate states, k, it can only be approximately treated. However, one may hope that the presence of large interactions with nearby excited states in the second part (such that $\tilde{\nu}_{kJ}$ is small) will dominate the entire B term. This was certainly the case in the cyclopropane study previously cited. The B term evaluation required the calculation of transition amplitude matrices among all pairs of 20 excited states, 10 of them degenerate. Each CI wave function was approximated by retaining the 640 largest terms in its configuration expansion; this comprised typically 95% of the norm of the wave function. One expects only small (10%) errors in one-electron matrix-element evaluation by this procedure.

Seamans and Moscowitz[20] have pointed out that, in certain point groups, approximate evaluation of the B term as a finite sum may be origin dependent. D_{2d} is not, however, one of these point groups.

The results of the one-electron matrix element calculation are shown in Table IV. Calculated quantities shown are the excitation energy, the spectral parameters, A, B, D, and the magnetic moment A/D (the units of these quantities are consistent with eq 1–5), the length form of the oscillator strength, and the values of $\epsilon(\tilde{\nu})$ and $\Delta\epsilon(\tilde{\nu})$ in l mol^{-1} cm^{-2}) at the maximum absorption for each state. The correlated ground-state energy is −116.0893 au, 0.2635 au below the SCF energy. This may be compared with Dykstra's[18] result of −115.9739 au, from an SCEP calculation with six frozen orbitals at a slightly different geometry. The configuration space in this calculation is considerably larger. Use of the gradient form of the dipole operator resulted in values of $\langle i|\bar{\mu}|j\rangle$ differing by 10–15% from the length-form value for the corresponding matrix elements. Only length-form values were used in Table IV. The quantities ϵ_{max} and $\Delta\epsilon_{max}$ were calculated using normalized Gaussian line shapes with assumed bandwidths (Γ_{FWHM}) of 3000 (for states 1^1E, 1^1B_2, and 2^1E), 6000 (3^1B_2), and 500 cm^{-1} (for the remaining optically allowed states, 3^1E, 2^1B_2, $4^1E + 5^1E$, and 6^1E). A glance at any one of the experimental spectra shows that the use of single Gaussian line shapes is not very accurate, but it gives a rough estimate of theoretical values that may be compared directly with experiment.

All B terms, with the exception of that for the 2^1B_2 state, are seen to be significant (the largest B term reported for cyclopropane[6] was 5.3×10^{-4}), some even quite large (e.g., the 3^1E state has $B(1^1A_1 \rightarrow 3^1E) = 10.56 \times 10^{-4}$ μ_B D^2 cm). In no case was the first part of the B terms significant, although it is included in the calculation (the largest was 0.2×10^{-4} μ_B D^2 cm). Further analysis of individual B term contributions revealed the interactions among the various excited states. The states are coupled as follows: 1^1E and 3^1B_2 mix with each other; 1^1B_2 and 2^1E interact quite strongly; and states 3^1E and 6^1E together interact with the group $4^1E + 5^1E$. The corresponding matrix elements in the B term (eq 4) represent essentially the entire B term for a given state. States 4^1E and 5^1E are calculated to be nearly degenerate (3.3-cm^{-1} separation). Were these states treated individually, they would have enormous B terms, nearly equal in magnitude but opposite in sign ($B(1^1A_1 \rightarrow 4^1E) = 0.182$ μ_B D^2 cm, $B(1^1A_1 \rightarrow 5^1E) = -0.184$ μ_B D^2 cm) 100 times larger than any other calculated B term. The physically correct approach is clearly to treat the 4^1E–5^1E group as if it were 4-fold degenerate.

One notes that all magnetic moments are, in absolute value, rather small, typically 0.1 μ_B. Since, as seen from Table III, the states 1^1E–6^1E arise from excitation from the degenerate 2e orbital to various nondegenerate orbitals, one might expect the magnetic moments of these states to be due principally to the angular momentum of the hole left behind in the 2e orbital. If allene were a truly linear molecule, the 2e orbital would in fact be a real π orbital (orbital designations σ, π, and δ are valid only for linear molecules) and would have a magnetic moment of exactly 1. However, the calculated magnetic moment is small, $\langle 2e_x|L_z|2e_y\rangle = -0.02$. A simple calculation shows this is due primarily to the delocalization of the 2e orbital along the entire molecule.

If we place hydrogen atoms 3 and 4 in the xz plane, the hydrogen atoms 1 and 2 in the yz plane, and denote the antisymmetric combinations as $H_{12} = (H_1 1s - H_2 1s)/2^{1/2}$, and similarly for H_{34}, with carbon 1 bonded to hydrogens 1 and 2 and carbon 2 etc., then we may form the symmetrized bond orbitals ϕ_1 and ϕ_2 (neglecting overlap):

$$\text{“}\sigma\text{”}\ \phi_{1x} = (C_3P_x + H_{34})/2^{1/2}$$
$$\phi_{1y} = (C_1P_y + H_{12})/2^{1/2} \quad (6)$$

$$\text{“}\pi\text{”}\ \phi_{2x} = (C_1P_x + C_2P_x)/2^{1/2}$$
$$\phi_{2y} = (C_2P_y + C_3P_y)/2^{1/2} \quad (7)$$

The “real” orbitals ψ_1 and ψ_2 will be a mixture of these.

$$\psi_1 \sim (1 - \lambda^2)^{1/2}\phi_1 + \lambda\phi_2 \quad (8)$$

$$\psi_2 \sim -\lambda\phi_1 + (1 - \lambda^2)^{1/2}\phi_2 \quad (9)$$

The coefficient λ is presumed to be small. Note that both ψ_{2x}

(20) Seamans, L.; Moscowitz, A. *J. Chem. Phys.* **1972**, *56*, 1099.

Table IV. Comparison of Theoretical and Experimental Data

calculated spectrum		spectral parameters (calcd)[a]				optical absorption (calcd)[b]		optical absorption (obsd)[c]		MCD (calcd)[b]		MCD (obsd)[d]		
state	$E-E_{gs}$, eV	A	B	D	A/D	f	ϵ_{max}	energy, eV	ϵ_{max}	$\Delta\epsilon_{max}$	shape	energy, eV	$\Delta\epsilon_{max}$	shape
1^1A_2	6.566							<6.45	<300					
1^1E	6.872	−0.282	1.940	3.033	−0.093	0.0791	5700	6.5–6.9 (6.70 max)	3200 (f = 0.03)	−2.07	B	6.5–6.9 (6.71 max)	−8.6	B
1^1B_1	6.921													
1^1B_2	7.445	0	−16.254	10.084	0	0.2847	20600	6.95–7.85 (7.23 max)	23000	12.43	B	7.1–7.5 (7.27 max)	19.0	B
2^1A_1	7.609							f = 0.34				7.2–7.5 (7.3 max)	−34.0	B? (see text)
2^1E	7.691	0.114	17.441	1.237	0.092	0.0361 f[7.4 – 7.7 eV] = 0.321	2600			−13.79	B	7.5–7.9 (~7.7 max)	−7	B
2^1A_2	7.822													
2^1B_1	7.854													
3^1E	8.200	−0.123	10.559	1.195	−0.103	0.0372	16000	8.02	12000	−59.8	B			
3^1A_1	8.314													
2^1B_2	8.339	0	0.626	0.880	0	0.0278	12000	8.15	10300	−3.2	B			
3^1A_2	8.416													
4^1E	8.4184	0.122	−16.495	0.620	0.1964	0.0198	8600	8.25	9200	~100	B			
5^1E	8.4185							8.32	8900					
3^1B_1	8.420													
4^1A_1	8.529													
6^1E	8.624	−0.054	5.029	0.577	−0.093	0.0189 f[8.2 – 8.62 eV] = 0.109	8000	8.38 f[8.0 – 8.4] = ~0.12	7500	−28.1	B			
3^1B_2	9.066	0	−1.689	30.190	0	1.038	30000	8.5–9.0 (8.58 max)	18000 (f ~ 0.5)?	~1	B			

[a] Units of A, B, and D are μ_B D^2, 10^{-4} μ_B D^2 cm, D^2, respectively (μ_B = Bohr magneton); A/D is the magnetic moment (in units μ_B). [b] Calculated ϵ_{max} and $\Delta\epsilon_{max}$ from normalized Gaussian line shapes. Assumed bandwidths were 3000 cm^{-1} (1^1E, 1^1B_2, 2^1E), 6000 cm^{-1} (3^1B_2), and 500 cm^{-1} (for the remaining allowed transitions). A magnetic field of 40 kg was used in the experiment and in the $\Delta\epsilon$ calculation. [c] Units of ϵ are L mol^{-1} cm^{-1}; experimental data from Rabalais et al. [d] Units of $\Delta\epsilon$ are L mol^{-1} cm^{-1} (H = 40 kG); experimental data from Fuke and Schnepp.

Table V. Molecular Orbital Coefficients

basic function		$1e_x$	$1e_y$	$2e_x$	$2e_y$
$1/2^{1/2}[H_1-H_2]1S$			0.4108		−0.1965
carbon 1	$1P_x$	0.0870		0.4924	
	$2P_x$	0.0409		0.1999	
	$1P_y$		0.5170		−0.1508
	$2P_y$		0.1773		−0.1815
carbon 2	$1P_x$	0.1916		0.4281	
	$2P_x$	−0.0142		0.2421	
	$1P_y$		0.1916		0.4281
	$2P_y$		−0.0142		0.2421
carbon 3	$1P_x$	0.5170		−0.1508	
	$2P_x$	0.1773		−0.1815	
	$1P_y$		0.0870		0.4924
	$2P_y$		0.0409		0.1999
$1/2^{1/2}[H_3-H_4]1S$		0.4108		−0.1965	

Table VI. Rydberg States of Allene

states	term value, cm^{-1} [a]	quantum defect	defect (Betts and McKoy[27])
$\pi \rightarrow 3s$	27 163	1.016	0.90
$\pi \rightarrow 4s$	13 036		
$\pi \rightarrow 3p\sigma$	20 559	0.690	0.53
$\pi \rightarrow 3p\pi$	20 627	0.694	0.54
$\pi \rightarrow 3d\sigma$	16 454	0.418	
$\pi \rightarrow 3d\pi$	15 067	0.301	
$\pi \rightarrow 3d\delta$	14 692	0.267	
all $\pi \rightarrow 3p$	20 605	0.692	
all $\pi \rightarrow 3d$	15 194	0.313	0.23

[a] Term values averaged over states by using ionization threshold of 80 800 cm^{-1}.

and ψ_{2y} have nodes along the z axis. Neglecting the effect of the hydrogen atoms and the two center terms, the magnetic moments for the two states are

$$\langle\psi_{1x}|L_z|\psi_{1y}\rangle \simeq (\lambda^2/2) + \lambda\,(1-\lambda^2)^{1/2} \quad (10)$$

$$\langle\psi_{2x}|L_z|\psi_{2y}\rangle \simeq [(1-\lambda^2)/2] - \lambda(1-\lambda^2)^{1/2} \quad (11)$$

In the absence of delocalization ($\lambda = 0$), one sees that the magnetic moment of the 1e (σ) orbital vanishes, and that of the 2e (π) orbital is $^1/_2$. However, even modest coupling drastically alters the situation. For $\lambda = 0.3$ ($(1 - \lambda^2)^{1/2} = 0.95$), the magnetic moments are reversed in order of magnitude: $\langle\psi_{1x}|L_z|\psi_{1y}\rangle = 0.35$, $\langle\psi_{2x}|L_z|\psi_{2y}\rangle = 0.15$. The MO coefficients of the 1e and 2e orbitals actually obtained from the SCF are shown in Table V. It is seen that there is significant delocalziation in both the 1e (σ) and 2e (π) orbitals. As one might anticipate, the 1e orbital has a rather large magnetic moment, $\langle e_x|L_z|1e_y\rangle = 0.3364$ and the 2e orbital's moment is correspondingly small.

Comparison between Experiment and Theory

In this point group, D_{2d}, the optically allowed transitions between the ground state (1^1A_1) and excited states are $^1A_1 \rightarrow {}^1B_2$ (polarized along the molecular axis) and $^1A_1 \rightarrow {}^1E$ (polarized perpendicular to the axis). We are also able to assign all the observable optical transitions in the 6.7–8.6-eV range as members of either $1^1A_1 \rightarrow n^1B_2$ (n = 1, 2, 3) or $1^1A_1 \rightarrow n^1E$ ($1 \le n \le 6$). The results are summarized in Tables III and IV. The four singlet states arising from the $\pi \rightarrow \pi^*$ (2e → 5e) excitation are calculated to be in order $1^1A_2 < 1^1B_1 < 4^1A_1 < 3^1B_2$, falling at 6.57, 6.92, 8.53, and 9.07 eV, respectively. As seen from Table III, these states, with the exception of 4^1A_1, are rather compact. All other excited states calculated are mixtures of excitations of the form $\pi \rightarrow$ (3s, 3p, 3d, 4s); while the $\pi \rightarrow \pi^*$ excitations are important in many of these states, all have appreciable Rydberg character, as seen from their large values of $\langle(x^2 + y^2)/2\rangle$ and $\langle z^2\rangle$ (Table III). The lowest excited singlet state is the optically forbidden 1^1A_2 state, calculated at 6.57 eV. Its forbidden nature is in accord with the very weak (ϵ <300 L mol^{-1} cm^{-1}) absorption on the gas phase below 6.45 eV.

6.5–6.9-eV Region. The observed optical spectrum[1,13,14] shows a weak ($f \sim 0.03$) absorption with partially resolved vibrational structure (λ_{max} = 185 nm or 6.70 eV). The band is rather broad ($\sim$3000 cm^{-1}) and the high-energy side is obscured by the strong absorption beginning at 180 nm. There are two states calculated in this band: the $1^1E(\pi \rightarrow 3s)$ state at 6.87 eV (f = 0.079) and the forbidden valence state 1^1B_1 ($\pi \rightarrow \pi^*$) at 6.91 eV. The MCD spectrum of Fuke and Schnepp[1] shows only a nondispersive signal with a positive B term. They performed a theoretical calculation in which the excited-state magnetic moment was found to be 0.5 μ_B. They argue that such a moment would give rise to an A term clearly visible in the MCD signal. We calculate a much smaller magnetic moment, 0.093 μ_B. On the other hand, we do calculate a significant B term of correct sign for this state, 1.95×10^{-4} D^2 μ_B cm. Using a single normalized Gaussian line shape to fit the absorption profile, from the values of A and B we calculate an essentially pure nondispersive MCD signal; the theoretical values of ϵ_{max} and $\Delta\epsilon_{max}$ of 5700 and −2.1 L mol^{-1} cm^{-1} are in reasonable agreement with the observed values of 3200 and −8.6 Lmol^{-1} cm^{-1}, recalling that fitting the absorption line shape with a single Gaussian is a gross assumption.

The 7.0–8.0-eV Region. The spectrum in this region exhibits a strong (ϵ_{max} 23 000 L mol^{-1} cm^{-1}) broad, diffuse absorption beginning at 180 nm (6.9 eV), rising to a maximum at 170.5 nm (7.27 eV), with perhaps two vibrational series of four or five members partially resolved. The absorption, still strong at 164 nm (ϵ 14 000 L mol^{-1} cm^{-1}), diminishes slowly out to 157 nm (ϵ 5000 L mol^{-1} cm^{-1}). One strong transition is calculated in this region. It is the 1^1B_2 ($\pi \rightarrow$ 3p) state at 7.45 eV (f = 0.285). It is nondegenerate and therefore has no A term. It is calculated to have a very large negative B term, -16.264×10^{-4} D^2 μ_B cm; this is clearly visible in the MCD. The calculated g factor, $\Delta\epsilon/\epsilon$ of 0.0053, is in good agreement with the experimental result of 0.0071 at the absorption maximum. Although the experimental and theoretical values for the oscillator strength suggest this is a valence state, the CI vector for this state is dominated by the $\pi \rightarrow$ 3p excitation, and the state is calculated to have a large spatial extent (Table III).

Another allowed, but weak, transition is calculated in this band. This is the $2^1E(\pi \rightarrow 3p_z)$ state at 7.69 eV (f = 0.037). The combined calculated strength for the two transitions (f = 0.322) is in excellent agreement with the experimental result of f = 0.34. The absorption due to the $1^1A_1 \rightarrow 1^1B_2$ transition buries the $1^1A_1 \rightarrow 2^1E$ transition. However, the MCD in the 164–157-nm region shows a distinct positive B term like band with a minimum at 160.5 nm ($\Delta\epsilon$ −7 mol^{-1} cm^{-1} at 7.7 eV). The origin of this band is in the 7.56–7.65-eV range. The 2^1E state is calculated to have a small magnetic moment (a small A term) and a very large positive B term, i.e., a nondispersive negative MCD signal. The calculated value of $\Delta\epsilon$ at the absorption maximum is −13.8 L mol^{-1} cm^{-1}, in good agreement with experiment.

There is one curious feature of the MCD spectrum in this region. A series of five narrow negative bands, beginning at 172 nm, with roughly 665-cm^{-1} intervals, appear with large intensity ($\Delta\epsilon_{max}$ −34). These bands do not correspond to any feature in the absorption spectrum or its derivative. It appears unlikely, therefore, that these bands are due to the 1^1B_2 state. Fuke and Schnepp[1] argue that this is a nondegenerate Rydberg transition; in fact, they tend to agree with Robin[5] that this is the other half of the 1^1E ($\pi \rightarrow$ 3s) state, which is a member of the series converging to the upper ionization threshold at 10.6 eV.

There is another possible explanation. We calculate another electronic state between the 1^1B_2 and 2^1E states; this is the optically forbidden 2^1A_1 ($\pi \rightarrow$ 3p) state at 7.61 eV. A degenerate e mode may vibronically couple the 2^1A_1 and 2^1E states. This type of coupling is apparently responsible for the strong MCD signal observed in the optically forbidden $^1A_{1g} \rightarrow {}^1B_{2u}$ transition of benzene.[21,22] A similar situation may prevail here. On the other hand, a Jahn–Teller splitting of the 2^1E state into two components at 7.3 and 7.55 eV may be responsible for the observed MCD. This calculation at the ground-state equilibrium geometry cannot rule out either of these possibilities. Experimental absorption and MCD spectra of perdeuterioallene (C_3D_4) in this region may be quite useful, as was the case in benzene.

The 8.0–8.5-eV Region. There are nine distinct electronic states calculated in this band, five of them allowed. In a 40-cm^{-1} band within this region, there are four electronic states, two of them ^1E states; the calculated ^1E states are split by 3.3 cm^{-1}. The seven lowest states all arise from the various $\pi \rightarrow$ 3d excitations.

The first state calculated in this band is the 3^1E ($\pi \rightarrow 3d_{z^2}$) state at 8.260 eV (f = 0.0372). The second and third states are the nearly degenerate $^1A_1$ and $^1B_2$ components of the $\pi \rightarrow$ 3d excitations. The forbidden 3^1A_1 state is at 8.314 eV; it has appreciable valence character ($|c|^2$ ($\pi \rightarrow \pi^*$) = 0.32). The 2^1B_2 state, at 8.339 eV (f = 0.0278), is essentially the $\pi \rightarrow$ 3d excitation. The next four states are calculated to fall within a 40-cm^{-1} band: (a) the 3^1A_2 ($\pi \rightarrow$ 3d) state at 8.416 eV; (b) the 4^1E ($\pi \rightarrow 3d_{x^2-y^2}$) (2e → 1b$_1$) state at 8.4184 eV ($f$ = 0.0096); (c) the 5^1E state ($\pi \rightarrow 3d_{xy}$) at 8.4188 eV (f = 0.0102); (d) the 3^1B_1 ($\pi \rightarrow$ 3d) state at 8.420 eV. The eighth state in this region is the valence 4^1A_1 ($\pi \rightarrow \pi^*$) state at 8.529 eV. Since it is orthogonal to the 3^1A_1 state, it must have significant Rydberg components ($|c|^2$ ($\pi \rightarrow$ 3d) = 0.33). The highest state in this band is the 6^1E ($\pi \rightarrow$ 4s) state at 8.62 eV (f = 0.0189).

The optical absorption spectrum of Rabalais et al.[13] shows five distinct peaks at 8.02, 8.15, 8.24, 8.32, and 8.38 eV; the intervals between maxima are 1046, 761, 4872, and 537 cm^{-1}. Rabalais et al. assign the entire series to the $^1B_2$ and ^1E ($\pi \rightarrow$ 3p) Rydberg states, coupled with a very anharmonic stretch, $\bar{\nu}_3$, which appears in the ground-state Raman spectrum at 1071 cm^{-1}. The spectrum

(21) Douglas, I. N.; Grinter, R.; Thompson, A. J. *Mol. Phys.* **1973**, *26*, 1257.
(22) Rosenfield, J. S.; Moscowitz, A.; Linder, R. E. *J. Chem. Phys.* **1974**, *61*, 2427.

is certainly suggestive of pure vibrational character, although such strong anharmonicity is not observed in the two lower absorption bands at 6.7 and 7.2 eV. Each of the observed absorption peaks is strong ($\epsilon_{max} \sim 10000$) but narrow ($\Gamma \sim 300$ cm^{-1}), with several subsidiary maxima separated by very low-frequency intervals.

We propose a different assignment. The plethora of calculated excited states in this region is the sharp contrast with the simple vibrational pattern suggested by the optical absorption spectrum (albeit with the invocation of strong anharmonicity). We assign the five distinct bands to individual electronic transitions; the peaks at 8.02, 8.15, 8.24, 8.32, and 8.38 are assigned to the states 3^1E, 2^1B_2, 4^1E, 5^1E, and 6^1E calculated at 8.20, 8.31, 8.34, 8.4184, 8.4188, and 8.62 eV, respectively. Although the calculated oscillator strengths for these transitions are small ($0.01 < f < 0.037$), the observed absorption profiles are narrow, and have small integrated intensity. The calculated oscillator strength for the entire band, $f = 0.109$, is in excellent agreement with our estimate of the experimental result, $f \sim 0.12$. We calculate the 4^1E and 5^1E states to be nearly degenerate. This may be an artifact of the calculation, since the basis set is deficient. The 4^1E state is primarily the $2e \rightarrow 1b_1$ excitation, and there is only one b_1 molecular orbital in this basis. On the other hand, a more refined calculation may not remove this near degeneracy. But it is not unlikely that the 13 potential surfaces in this 0.5-eV region interact strongly with each other to give rise to what coincidentally appears to be a simple vibrational structure. The calculated MCD spectrum is quite striking. Three strong distinct bands are predicted. The first, due to the $1^1A_1 \rightarrow 3^1E$ transition at 8.20 eV (calcd), is a very strong positive *B* term like band ($\Delta\epsilon_{max} \sim -60$ L mol^{-1} cm^{-1}). The high-energy side may contain a weak ($\Delta\epsilon_{max} \sim -3$ L mol^{-1} cm^{-1}) B term like band due to the 2^1B_2 state calculated at 8.34 eV. The second band, due to the 4^1E and 5^1E states, is even more intense. It will also be negative *B* term like, with one or perhaps two large positive MCD bands, with $\Delta\epsilon_{max} \sim 100$ L mol^{-1} cm^{-1}. The third band is due to the $1^1A_1 \rightarrow 6^1E$ transition; it, again, consists of a large positive B term and is calculated to have a large negative MCD ($\Delta\epsilon_{max} \sim -28$ L mol^{-1} cm^{-1}). It should be emphasized that these three distinct features are all predicted to lie in the relatively narrow 155–148-nm range. The crude assumptions used to calculate the theoretical spectrum do not lend themselves to quantitative results. But the qualitative predictions are clear: three large distinct MCD bands, all nondispersive, alternately negative, positive, and negative, roughly corresponding to the absorption profile. Experimental observations that deviate from this may be useful in determination of the state ordering within this band and the extent to which the various surfaces interact among themselves.

The 3^1B_2 ($\pi \rightarrow \pi^*$) State. This state is of clear valence nature in this basis. It is calculated to be at 9.06 eV ($f = 1.038$). Although Rauk et al.[10] assign this to the diffuse band starting at 8.78 eV in the spectrum of Iverson and Russell,[14] it appears to us that in the spectra of both Iverson and Russell et al. and Rabalais et al.[13] the 3^1B_2 state is responsible for the strong broad absorption beginning at 8.58 eV. Although the calculated oscillator strength agrees with the experimentally observed strong absorption in this region ($7000 < \epsilon < 17000$ over a broad range), the energy of this state is calculated 0.48 eV too high compared to experiment. Even the admission of the 8.78-eV figure leaves an unacceptable discrepancy between theory and experiment for such an excited state and is significantly larger than errors apparent in other excited state obtained by this calculation. However, a similar problem exists in the calculation of the lowest valence ^1B_u state of 1,3-*trans*-butadiene. This strongly allowed state is observed at 5.95 eV.[23,24] Using GVB-CI techniques and a similar basis set, Nasciemento and Goddard[25] calculate this state at 7.05 eV (vertical). They call this state "the most serious challenge to the theoretical description of the electronic states of polyenes". It is not at all unlikely that the valence $^1B_2$ ($\pi \rightarrow \pi^*$) excited state of allene presents similar problems. The investigation of this state may require much more extensive basis functions[17] and calculations at nonvertical geometries,[25] techniques not intended to be part of this calculation.

The Rydberg Spectrum of Allene. Essentially all previous attempts[5,10,12-14,26,27] to unravel the absorption spectrum of allene have rested upon the formation of appropriate Rydberg series leading up to one or two thresholds within the first ionization band. The presence of many complex bands with apparent vibrational structure has been a major stumbling block in the analysis of the spectrum. Both Rabalais et al.[13] and Betts and McKoy[26] (who calculated the Rydberg series using a Pseudopotential method) quote Herzberg:[27] "Some of these series are fragmentary and probably represent simply vibrational members of the main Rydberg bands". Betts and McKoy and "We can account for all the observed Rydberg transition in allene if we assume that some of the observed bands are vibrational...". And Iverson and Russell[14] state "We have presently located at least four diffuse bands that do not appear to be either Rydberg or vibrational in character" (at 6.72, 7.30, 8.20, and 8.78 eV).

Our assignment of the absorption spectrum is based on an examination of the computed spatial extents and leading terms of the configuration expansion of the various excited states. It seems to us that there are two principle mistaken assignments that lead to the aforementioned difficulties. First, the strong transition ($1^1A_1 \rightarrow 1^1B_2$) at 7.23 eV is identified by all previous authors as the $^1B_2$ component of the $\pi \rightarrow \pi^*$ excitation. In view of the large oscillator strength ($f = 0.34$), this is quite reasonable. However, one sees from Table III that this state is primarily the $\pi \rightarrow 3p$ excitation with significant valence character. Both its spatial extent and term value (23 000 cm^{-1}) are consistent with excitation to a 3p Rydberg orbital. The usually large oscillator strength is due to significant $\pi \rightarrow \pi^*$ mixing. As previously discussed, we prefer to assign the $\pi \rightarrow \pi^*$ excitation to the strong band whose onset is at 8.58 eV. This clears up another mystery. Robin[5] says "unlike the situation in ethylene and butadiene, in which methylation moves the long-axis allowed $\pi \rightarrow \pi^*$ band rapidly to lower frequencies, that of tetramethyl allene (59140 cm^{-1} vertical) is actually somewhat higher than that of allene (58000 cm^{-1} vertical)." The assignment of the $\pi \rightarrow \pi^*$ band in allene to the transition at 69 200 cm^{-1} clearly eliminates this puzzle. Furthermore, this assignment makes sense in view of the fact that the $\pi \rightarrow \pi^*$ band in carbon suboxide (O=C=C=C=O) is observed[28] at 63 300 cm^{-1}.

The second problem is the assignment of the band at 8.02–8.38 eV, which is highly suggestive of vibrational structure. This band is variously assigned as pure $\pi \rightarrow 3p$ Rydberg or overlapping $\pi \rightarrow 3p$ and $\pi \rightarrow 3d$ Rydberg excitations. We find this band to be due to the $\pi \rightarrow 3d$ and $\pi \rightarrow 4s$ Rydberg excitations. The term values, 13 200–16 100 cm^{-1}, are slightly larger than usual for 3d Rydberg states, but not unusually so. In both *cis*- and *trans*-1,2-dimethylethylene, 3d term values of 15 100 and 15 270 cm^{-1}, respectively, are observed.

When these assignments are made, the rest of the spectrum falls easily into place. Incorrect assignment of these lower members of the Rydberg series naturally leads to difficulties at higher energies. Of course, the most significant test of Rydberg character is the existence of higher members of the series. We have calculated quantum defects for the $\pi \rightarrow ns$, $\pi \rightarrow np$, and $\pi \rightarrow nd$ series on the basis of our theoretical results. The experimental threshold of 10.02 eV was used. Taking into account the fact that our excitation energies are, in general, too high (probably due to a relatively low ground state), we lowered all calculated transition energies by 1800 cm^{-1}. Since the splitting of the various symmetry components of $2e \rightarrow ne$ excitations should

(23) Mosher, O. A.; Flicker, W. M.; Kuppermann, A. *J. Chem. Phys.* **1973**, *59*, 6502; *Chem. Phys.* **1978**, *30*, 307.
(24) Jones, L. C.; Taylor, L. W. *Anal. Chem.* **1955**, *27*, 228.
(25) Nasciemento; M. A. C.; Goddar, W. A., III. *Chem. Phys.* **1979**, *36*, 147; **1980**, *53*, 251.
(26) Betts, T. C.; McKoy, V. *J. Chem. Phys.* **1974**, *60*, 2947.
(27) Herzberg, G. "Molecular Spectra and Molecular Structure. Vol. III. Electronic Spectra and Electronic Structure of Polyatomic Molecules"; Van Nostrand: New York, 1967; p 541.
(28) Robin, M. B., ref 5, p 205.
(29) Robin, M. B., ref 5, p 24.

diminish higher in the Rydberg series, we averaged together the excitation energies for all the symmetry components arising from an individual 2e → *n*e excitation. The results are shown in Table VI. While the splitting among the 3d members is less than that in the 3p states, in neither case is the designation (σ, π, δ) (e.g., 3pπ) valid, as it would be in the case of a linear molecule. In addition, the $\pi \rightarrow 3p\pi$ "state" is slightly lower than the $\pi \rightarrow 3p\sigma$ "state", due to valence $\pi \rightarrow \pi^*$ mixing in the 1^1B_2 state. In the d series, we have $\sigma < \pi < \delta$ as in the usual case, although these are not "good" quantum numbers. Similar averaging over the states designated σ, π, δ, etc. lead to the calculated quantum defects, $\delta_s = 1.016$, $\delta_p = 0.0692$, and $\delta_d = 0.313$. These are quite reasonable values, although the value of δ_d is larger than is typically the case. However, one must keep in mind that these defects are calculated from the lowest members of the various Rydberg series, and allene is large enough so the lower Rydberg states may lie significantly below the strictly hydrogenic value. Nonetheless, even under such gross assumptions, in every case, peaks in the absorption spectrum are observed (±200 cm^{-1}) where predicted by the Rydberg formula

$$E_n = I - R/(n - \delta)^2 \qquad (12)$$

for each of the series, s, pσ, pπ, dσ, dπ, and dδ through $n \simeq 6$, or 3200 cm^{-1} below the ionization limit. This then seems to provide some real basis for our assignments.

Conclusion

We have calculated the vertical singlet excited states of allene in the 6.5–8.6-eV range. All optically allowed states in this region arise from valence → Rydberg excitations, with the exception of the valence $\pi \rightarrow \pi^*$ transition, which we assign to the band at 8.58 eV (9.06 eV calcd). Calculated oscillator strengths and excitation energies are consistently in good agreement with experiment. In addition, we have calculated the theoretical MCD parameters A and B for all the excited states in this region. All degenerate ^1E states are found to have small magnetic moments. The magnetic moment of the highest filled 2e orbital is also small, due to delocalization effects. All optically allowed excited states (except the 2^1B_2 state at 8.34 eV) have large B terms. Therefore, all of these states, degenerate or not, would show a nondispersive MCD signal (i.e., would appear nondegenerate). The theoretical MCD spectrum also is in agreement with experiment; the only unexplained feature in either the absorption or MCD spectra (the narrow bands beginning at 172 nm) is probably due to vibronic coupling between the 2^1A_1 and 2^1E states or Jahn–Teller splitting of the 2^1E state itself. The four singlet states arising from the $\pi \rightarrow \pi^*$ excitation are in order $1^1A_2 < 1^1B_1 < 4^1A_1 < 3^1B_2$. All other states in this region are $\pi \rightarrow$ Rydberg excitations. The resulting analysis of the Rydberg series leads to reasonable quantum defects. Higher members of each Rydberg series are found in the absorption spectrum. Outside of the observed MCD at 7.3 eV, it does not appear to be necessary to include the effects of nonvertical geometries in order to interpret either the absorption or MCD spectrum of allene.

Acknowledgment. We gratefully acknowledge the support of the National Science Foundation, Grant CHE-81-06016.

Registry No. Allene, 463-49-0.

S_N2 Reactions in the Gas Phase. Temperature Dependence of the Rate Constants and Energies of the Transition States. Comparison with Solution

Gary Caldwell, Tom F. Magnera, and Paul Kebarle*

Contribution from the Department of Chemistry, University of Alberta, Edmonton, Alberta, Canada T6G 2G2. *Received March 28, 1983*

Abstract: The rate constants for the gas-phase reactions $Cl^- + RBr = ClR + Br^-$, where R = Me, Et, *n*-Bu, *i*-Pr, and *i*-Bu, were determined for temperatures between 25 and 390 °C with a pulsed electron beam high ion source pressure mass spectrometer. The rate constants for Me decreased with an increase of temperature (negative temperature dependence). Et and *n*-Bu had almost no temperature dependence while *i*-Pr and *i*-Bu had positive temperature dependence. An analysis of the data on the basis of theory provides approximate values for ΔE_0, the energy of the transition state

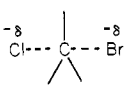

relative to the energy of the reactants. These ΔE_0 values are as follows: Me, −2.5; Et, 0.8; *n*-Bu, −0.5; *i*-Pr, +5.1; *i*-Bu, +5.7 kcal/mol. The $\delta\Delta E_0$ are compared with relative activation energies: δE_a in solution (C. K. Ingold and A. J. Parker) and calculated strain energies $\delta\Delta E_{strain}$ due to steric repulsions in the transition state (C. K. Ingold and D. F. DeTar). An approximate agreement between the three sets of data is found. This finding supports the assumption of Ingold that steric effects in the transition state dominate the relative rates of this reaction series. The temperature dependence of the rate constants in the gas phase is of interest to ion–molecule reaction theory. It provides a graphic demonstration for the effect of the central barrier in the double-well reaction coordinate. When ΔE_0 is negative, negative temperature dependence is observed. When $-\Delta E_0$ is small (Me, *n*-Bu) the reaction proceeds with chemical activation at the very low pressures used in ion cyclotron resonance but with near Boltzmann transition-state distribution at the higher pressures used in high-pressure mass spectrometry. When ΔE_0 is positive, the reaction proceeds with positive temperature dependence and boltzmann transition-state distribution.

Studies of the kinetics and mechanism of bimolecular nucleophilic S_N2 reaction 1 have played a fundamental role in the development of physical organic chemistry.[1-5] Many aspects of the structural and solvent effects in protic and aprotic solvents

0002-7863/84/1506-0959$01.50/0 © 1984 American Chemical Society